Eur. Phys. J. D **44**, 239–247 (2007)
DOI: 10.1140/epjd/e2006-00175-2

THE EUROPEAN PHYSICAL JOURNAL D

Update on ignition studies at CEA

P.A. Holstein[a], M. Casanova, A. Casner, C. Cherfils, E. Dattolo, L. Disdier, D. Galmiche, J. Giorla, M. Houry, J.P. Jadaud, S. Laffite, S. Liberatore, P. Loiseau, L. Lours, L. Masse, M.C. Monteil, O. Morice, M. Naudy, F. Philippe, F. Poggi, F. Renaud, G. Riazuelo, Y. Saillard, P. Seytor, M. Vandenboomgaerde, and F. Wagon

CEA/DAM/Ile de France, B.P. 12, 91680 Bruyères-le-Chatel Cedex, France

Received 21 December 2005 / Received in final form 11 April 2006
Published online 28 July 2006

Abstract. This article sums up the theoretical and experimental studies about ignition. Three experiments are salient this year on the Omega laser in collaboration with DOE laboratories (1) 3 cones of beams allow to mimic the LMJ configuration and to get symmetry measurements. (2) We measured perturbations due to hydro-instability in CHGe planar samples with face-on and side-on radiographs. (3) We improved our nuclear diagnostics, particularly the neutron image system tested on direct drive implosions. As far as LMJ target design is concerned, we defined a preliminary domain corresponding to the possible operation at 2ω. At 3ω we studied the low mode instability effects on the DT deformation (due to the laser or to the target) and on the yield. The stability is clearly improved with graded doped CH for our nominal capsule L1215.

PACS. 52.57.-z Laser inertial confinement – 52.57.Bc Target design and fabrication – 52.57.Fg Implosion symmetry and hydrodynamic instability

1 Introduction

The objective of the ICF Program at CEA is to burn cryogenic DT capsules indirectly driven with the Laser Megajoule (LMJ) [1]. We plan to have significant experiments at the beginning of the next decade [2].

About laser plasma interaction we are preparing the LIL experiments (1 quad of 4 beams, LMJ prototype) to validate the effect of the "longitudinal smoothing" on beam deflection for example. For the theoretical point of view we implemented a Stimulated Brillouin Scattering package in the paraxial propagation code Hera which is a platform with full hydrodynamics 2D/3D. The first applications of this code are in progress.

For the time being we have some experiments on the Omega laser in collaboration with DOE laboratories. As far as symmetry is concerned we got some foam ball radiographies with 3 cones of beams in order to reproduce the LMJ cone angle viewed from the capsule. To study the hydro instabilities we measured perturbations in CHGe planar samples with face-on and side-on radiographies. The initial perturbations can be imposed on the front surface or on the rear surface.

About the target design for LMJ [1] we studied various enlargements of the operational domain by using our global modeling. First of all we improved this modeling, particularly the laser-plasma instability safety factor. (1) We define a domain corresponding to the possible operations of LMJ at 2ω in the range 2–3 MJ. (2) At 3ω our nominal target is still L1215 at radiation temperature 300 eV. For it we give some results of the deformations due to the low modes cumulated from the different sources: irradiation non-uniformities, capsule defects and random experimental variations within the LMJ specifications. (3) We made some multimode simulations of our nominal capsule L1215 with graded doped CH and compared to LLNL results: the roughness limit to get a high yield is multiplied by more than 3.

For several years we have developed and tested a penumbral neutron image system: today we are confident to get the right resolution and the right sensitivity for LMJ conditions.

2 Experiments to prepare ignition

2.1 Laser-plasma interaction

In a hohlraum different issues are related to the laser plasma interaction: the most concerning are the backscatter of the laser light and the beam deflection but the laser beam smoothing can greatly mitigate these effects [3]. In order to prepare LMJ experiment we must check that the beam smoothing is efficient enough to control the beam deflection. That is why on LIL (LMJ prototype) we planned an experiment called "window crossing" in order to measure the beam deflection for different angle of the beam corresponding to the LMJ beam angles (Fig. 1).

[a] e-mail: holstein@cea.fr

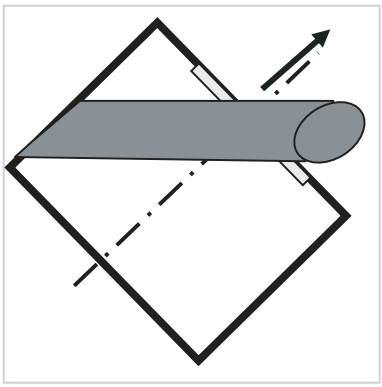

Fig. 1. "Window crossing" experiment on LIL aimed at measuring the beam deflection. The hohlraum dimensions are $\varnothing = 4$ mm, $L = 2$ mm.

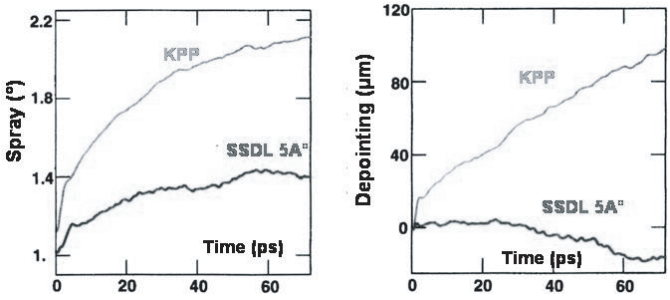

Fig. 2. Parax code results: beam spray at the left and beam depointing at the right in presence of different smoothings (grey curve for KPP only, black curve for "longitudinal SSD" with 5 A° band width) at the end of the laser pulse ($t = 3$ ns) during a smoothing cycle 70 ps.

Indeed the filamentation of the laser beam in a plasma results in a beam spray and in a beam deflection (the latter is due to the velocity perpendicular to the beam axis, shown by the arrow in the figure). In a hohlraum these phenomena occur in the neighbourhood of the laser entrance hole.

Here we are going to show some results for the intermediate cone angle of LMJ, 49°, the intensity is 1.8×10^{15} W/cm^2, the pulse shape is square, 3 ns in duration. We used a chain of 2 codes to simulate this experiment: a hydrodynamic code and a paraxial code for the propagation of the laser beam. A 2D hydrodynamic simulation gives us the plasma features during the laser pulse. At the end of the pulse, the electronic density Ne along the beam varies from 2%Nc to 25%Nc, the electronic Te is ∼3 keV and Ti ∼1 keV. This experiment allows to validate our codes in conditions of Ne, Te and Ti of the same order of magnitude as for LMJ target and to extrapolate to the true LMJ conditions.

We used our paraxial code "Parax" [4] with these plasma features in order to simulate effect of different smoothings (spatial smoothing only with KPP or spatial and temporal smoothing by using KPP and longitudinal Smoothing by Spectral Dispersion (SSD) as planned for LMJ (1). As it is not possible today to get such a simulation for the whole pulse with a reasonable CPU time, we chose to simulate the propagation at 3 different times during the pulse: during the Parax simulation the hydro is unchanged and here correspond to the end of the pulse. The deflection and the spray are given after 70 ps of interaction because this is the SSD period and we think that the equilibrium state is reached. The spray is the RMS of the ray angles with respect to the mean value (it is quasi–symmetric with respect to the beam axis). The deflection is characterized by the depointing on the wall of the hohlraum.

In Figure 2 we can conclude that the beam spray and the beam depointing (or deflection) are immediately reduced by adding the SSD. The same simulation at the beginning of the pulse shows that the effects are qualitatively the same.

The paraxial codes are essential tools to interpret laser plasma interaction and the effect of the smoothing as we have just shown. At CEA we have been implementing a paraxial propagation package in a full hydrodynamic code in order to overcome Parax code limitation, namely to use a frozen hydro state and to calculate only the density fluctuations associated with the filamentation. This Eulerian code called "Hera" is an "adaptive mesh refinement" Eulerian code and it is used only with mass and momentum equations for now (internal energy equation requires too much CPU time for the first applications but it is going to be used in the mid term). Hera code deals with the backscatter Brillouin wave with an implicit scheme which allows moderate time step. This code is similar to the code pF3D of LLNL but the harmonics and sub-harmonics of the ion acoustic wave associated to the Brillouin are included in the code: indeed, they can be a source of backscatter saturation.

2.2 Hohlraum physics

We had several campaigns of shots on the Omega laser about hohlraum physics. We have a good agreement for the radiative temperature between our FCI2 simulations [5] and Dante [6] or DMX [7] measurements (broad band spectrographs) if we take into account the backscatter ∼5%, but for the 22° cone the backscatter is higher ∼8%.

These 3 last years we focused our experiments on symmetry studies with 3 cones of beams mimicking the LMJ configuration. We measured the shock front radius inside a foam ball by radiography [8]. In Figure 3: we can compare the mean motion of shock front radius for different campaigns versus time with a generic simulation: the agreement is satisfactory.

The mode 2 deformation is compared with a simulation for the 2004 campaign (Fig. 3b): it is in the range ± 1 μm, which is small because the beam pointing was optimized to minimize the deformation. The experimental points correspond to the average of the 4 images of the same track of the gated camera and the error bars corresponds to the dispersion of these 4 images. For the 3 first

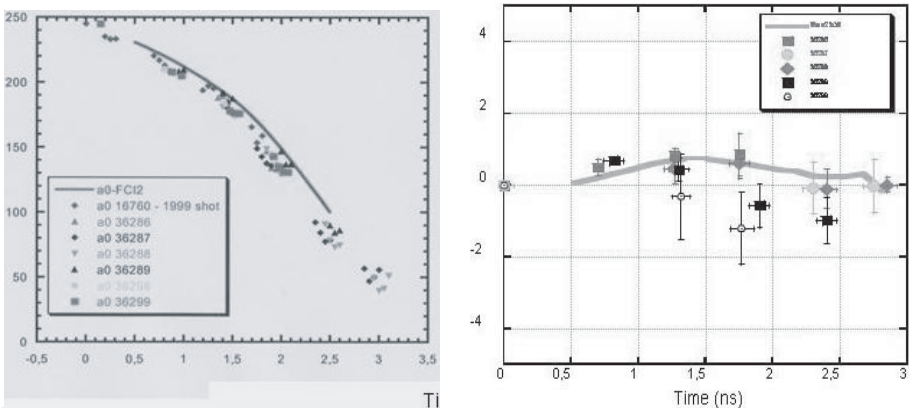

(a) (b)

Fig. 3. (a) The mean radius of shock front is compared versus time to a 2D simulation (solid line) for 3-cones experiments. (b) The mode 2 deformation of the foamball for the 2004 campaigns of shots compared to a simulation (solid line).

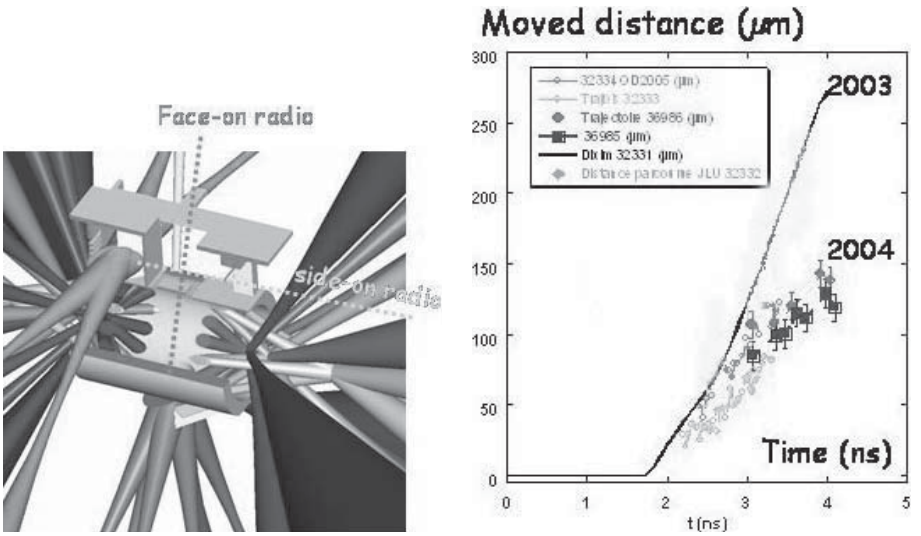

(a) (b)

Fig. 4. View of the target and the laser beams (the heater beams are in (a) and (b), the beams for face-on radiography come from the bottom, the beams for the side-on radiography come from foreground). (b) The foil motion versus time for different campaigns of shots and the solid line is a 2003 simulation.

shots the agreement for mode 2 is very good at any time, for the 2 others the image the quality is less good but the disagreement could come from experimental random variations as well: laser pointing, beam imbalance, ... For the mode 4 deformations (not shown) the conclusion is not as clear as for mode 2. It could be a diagnostic issue (we reached the limit of the capability of the diagnostic) or a simulation issue (it doesn't reproduce all the aspects of the symmetry). The kind of agreement obtained here is about the same as LLNL's one [9].

This year and for the future we are going to image the core (D2 seeded with Ar) at stagnation time for which the convergence is larger and the deformation as well, so easier to measure.

2.3 Capsule physics

As far as the capsule physics is concerned our main effort is about the study of hydrodynamic instability on Omega. A corrugated foil placed on the hohlraum wall is accelerated by the radiation: the perturbations are measured by means of the transmission of a X-ray source through the foil (a face-on radiography) [3]. In Figure 4a we can see a 3D scheme of the target and of the laser beams: this experimental set-up is similar to the set-up used at Nova with only one radiography measurement at once [10]. The originality of this experiment is to use 2 radios on each shot so we measure the foil motion with side-on radio and the perturbation amplitude with the face-on radio. We measure also the radiative temperature through the laser entrance hole with Dante (T_r max $\sim$180 eV): we have a good agreement between the measurement and the simulation of the hohlraum alone within $\pm 3\%$. On the other hand we made simulations of the foil alone irradiated by X-rays with the temperature deduced from the previous simulations (lower than Dante T_r measured through the holes) in order to calculate the foil motion and the perturbation growth.

In order to study LMJ target ablator the foil is made of CHBr (2.5% Br in atoms) and the laser pulse is composed of a 1ns plateau and a 1ns main pulse, the total duration is 2.5ns.

In Figure 4b the foil motion versus time is given. We state that we had a strong discrepancy between the 2003

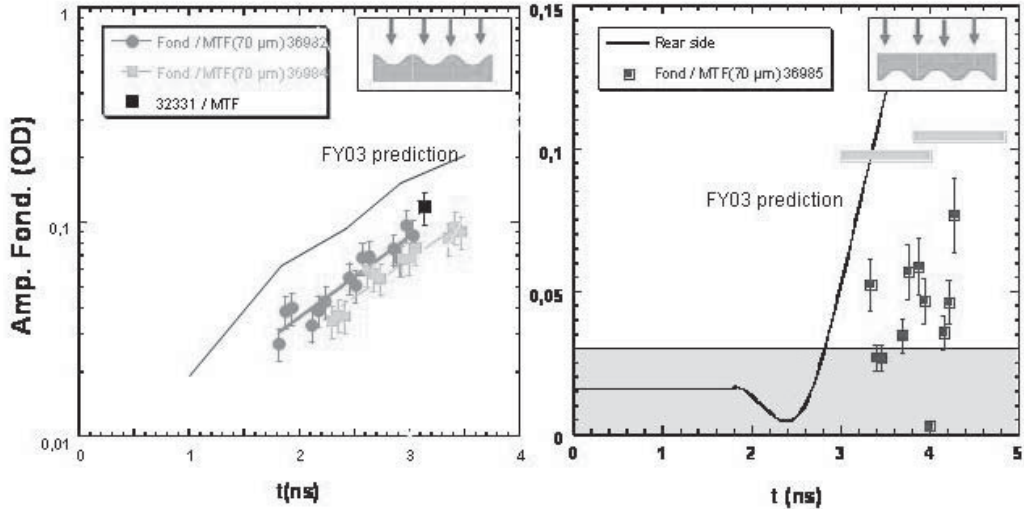

Fig. 5. On the left, perturbation amplitudes versus time for a front initial corrugation. On the right, perturbation amplitudes versus time for a rear initial corrugation: the grey region correspond to the experimental noise.

code prediction and the 2004 experimental points. We will discuss this point at the next paragraph after having shown the perturbation results.

The goal of this experiment is also to compare the amplification of an initial corrugation at the front or at the rear of the foil. Indeed, in the LMJ capsule there is some transmission of the perturbations from the DT roughness toward the ablation front, called feedthrough. In this experiment the wavelength of the corrugation is 70 μm (50 μm was also used but not shown here). In the Figure 5 you can see the perturbation amplitude versus time for initial corrugation at the front (left figure) or at the rear (right). For the front corrugations measured in 2004, we observed less amplification than expected (FY 2003 prediction). It is consistent with the Figure 4 measurements of the foil motion. For the rear corrugation, the perturbations are very small on the image, so we need to understand the front corrugation growth in the first place.

Both discrepancies between code and experiment in motion and in perturbation can be explained if the foil is not irradiated with the radiative temperature deduced from the measurement that we used in our simulations (we must cut down T_r by 15% to restore the agreement). One of the possible explanations is a "closing" of the hohlraum so the foil receives less radiation than simulated: the 2005 experiment is aimed at clearing this point by a direct measurement of the X-ray intensity irradiating the foil with DMX and the shock velocity measurement in the foil.

3 Target design for LMJ

The perturbations of the capsule are classically divided in spherical harmonic modes (or Legendre modes), more specifically in high modes (>10) and low modes for physical reasons and numerical reasons (the numerical simulations to calculate them are different). Indeed, the high modes are calculated in a wedge of the sphere (15–30°), are only due to the capsule defects and can enter the nonlinear regime. The low modes have initially a much larger amplitude so they can hide the high modes, the low mode come also from the irradiation non-uniformities and they stay in the linear regime.

3.1 Capsule ablator with an graded dopant

During an implosion there are several locations of instability: (1) during the acceleration stage, the ablation front and the ablator/fuel interface (the fuel becomes denser that the ablator). (2) during the deceleration, there are instabilities at the central hot spot and at the ablator/fuel interface (for the interface this is mainly because of the convergence). The dopant in the ablator is necessary to increase the opacity and to protect the fuel from preheating, but it increases the ablation-front instability growth. It has been shown by LLNL [11] that a graded dopant (Cu) in Be for the nominal NIF design (NIF-PT) allows to increase the limit roughness that a given capsule can bear.

We made some simulations of multimode perturbations (modes 12-120) of our nominal capsule L1215 made of CH doped with Ge [1]: in Figure 6 the graded dopant capsule (made by 4 layers shown in the figure) has a limit roughness of 280 nm (for 75% of nominal yield) instead of 60 nm for the uniform dopant (0.4% Ge). The graded dopant multiplies the limit roughness of L1215 capsule by ∼4–5 which is the same order of magnitude as the factor obtained by LLNL (the results are shown in the same figure for the capsule made of ablator 160 μm / fuel 90 μm optimized by Herrmann [11]). But the comparison is only qualitative because the capsules are close but not identical (the dopant concentrations are the same, not the thicknesses) and the simulation conditions are also different.

The round point in the figure at 100 nm is obtained by adding a 2 μm DT roughness to the ablator roughness: the difference is small.

With graded dopant we observe the decrease of perturbation at the interface CH/ DT and the decrease of the high modes at the hot spot (modes > 60). The perturbations of the CH/DT interface for our nominal design are the most dangerous, the final effect of the graded dopant

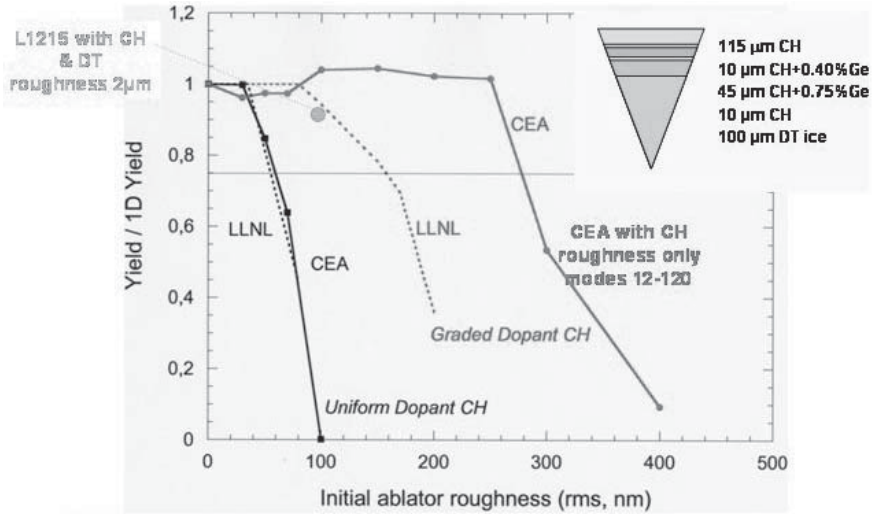

Fig. 6. The graded dopant multiplies the limit roughness of L1215 capsule by ∼4–5: solid line L1215 capsule, dashed curve, LLNL "new design" (see the text).

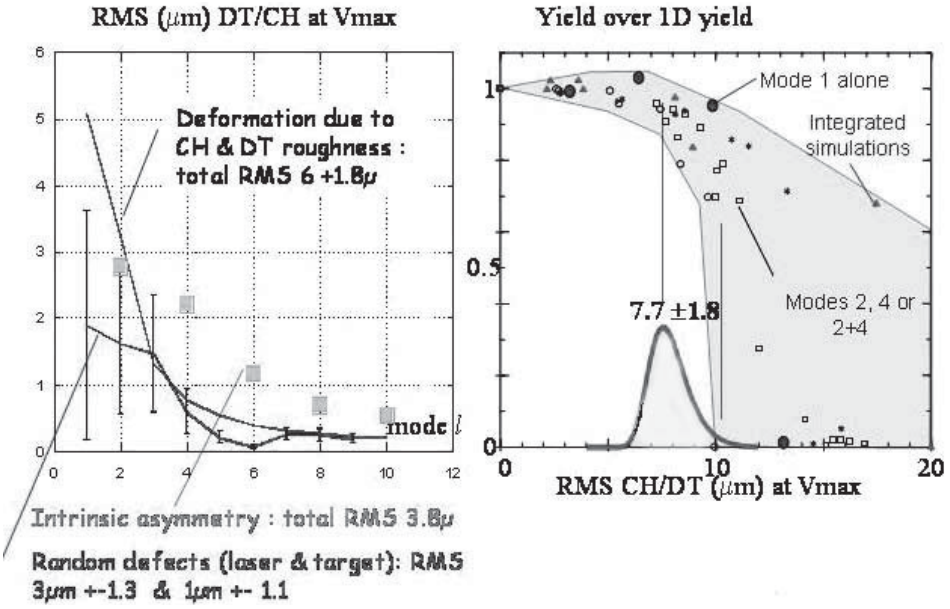

Fig. 7. On the left the 3 contributions to the DT deformation at max velocity on the right, the yield versus the total deformation with a Gaussian distribution due to the random variations (thick curve).

is favorable. But, surprisingly, the final spectrum of perturbations depends on the initial RMS for the same initial spectral shape.

Finally, the main effect of graded dopant observed in simulations is the following: a non-doped ablator layer adjacent to the fuel reduces the density jump at this interface and minimizes the perturbation growth at the end of the acceleration.

3.2 Low modes effect on symmetry

Here we focus on the low mode perturbations of the capsule deformation which in fact come from 3 contributions:

- the CH and DT initial defects (or roughness);
- the intrinsic irradiation asymmetry mainly due to the shape of the hohlraum which is cylindrical;
- the random experimental variations of the laser or the random variations of the target.

We calculate the 3 contributions separately with simulations or with a chain of codes-&-models and we add them quadratically considering that they are randomly distributed.

The growth of the initial defects of the capsule is calculated with capsule–only simulations of the hydro-code FCI2 mode by mode: the initial spectrum used is the NIF standard [12]. The final deformations of the CH/DT interface are taken at the maximum velocity. They are shown in Figure 7-left as a function of the mode number: we state that all the contributions decrease with mode number.

(1) For the CH and DT roughness the RMS cumulated for all low modes of the capsule is 6 μm due to CH defects and 1.8 μm due to DT roughness (the mode 1 is the largest ∼5 μm).
(2) The intrinsic asymmetry due to radiation (square in Fig. 7) is calculated with capsule-integrated hohlraum simulations of the code FCI2: only the even modes are

present and the maximum is ∼3 μm for mode 2. The cumulated RMS is 3.8 μm.

(3) The random variations from laser are due to the imbalance between the quads or due to their pointing. We assumed a Gaussian statistics with the LMJ specifications: 5% RMS/quad for the max power and 50 μm RMS/quad in pointing. We used a chain of models and codes to calculate them [1]. The random variations from the target are due to the capsule position in the hohlraum, off-centring of the laser entrance hole, ..., all of them with a 10 μm RMS. In Figure 7-left you can see the mean value of the laser-&-target variations and the error bars correspond to the RMS of the distribution. The cumulated RMS of all low modes due to the laser variations was 3 μm ($\pm$1.3 μm due to the statistics) and due to the target variations it was 1 μm ($\pm$1.1 μm).

The total of the cumulated RMS of all the sources is 7.7 μm ($\pm$1.8 μm) of DT outside surface deformation at maximum velocity.

To calculate the yield we used a large variety of simulations, capsule-only simulations (for which we imposed a non-uniform irradiation for a sample of modes) or integrated simulations (capsule + hohlraum): we guess that the curves yield-versus-deformation at Vmax are close from each other whatever the source of initial perturbation. From all these yield points emerges a region (in grey in Fig. 7-right and which becomes larger near the threshold because of the uncertainty) which gives an order of magnitude of the yield. In Figure 7-right we superimposed to this "yield region" and the DT deformation obtained previously. With the mean value of deformation (7.7 μm) the yield is quasi nominal but the tail of the distribution (∼10 μm) could be in the ignition threshold for which there is a strong uncertainty. If we don't take into account the mode 1 the total deformation is 5.1$\pm$1.1 μm, so that we get a gain for all the deformations. Moreover, the mode-1 simulations are difficult to make with an Lagrangian code, so the result is inaccurate for this mode.

All these results have been obtained with 0.3 mg/cc DT gas density, with 0.5 mg/cc (see Sect. 3.4) the robustness is under study but we know that it is degraded.

3.3 Preliminary domain at 2ω

To determine the domain of targets possible for LMJ we used our global modelling with different safety factors [1]. There are different ways to plot the operative domain (E, P) for LMJ, depending on the parameters kept constant: usually [1] we kept constant the ignition safety factor S_{ign} = 1.25 and the symmetry factor R_{ac} = 3.6 (S_{ign} = kinetic energy of the capsule / kinetic energy at the threshold and R_{ac} = spherical equivalent hohlraum radius/ capsule radius).

In order to generalize the domain from 3ω to 2ω we keep constant the initial aspect ratio of the capsule and the symmetry factor, the ignition safety factor can be changed. Moreover, for each target, we calculate safety

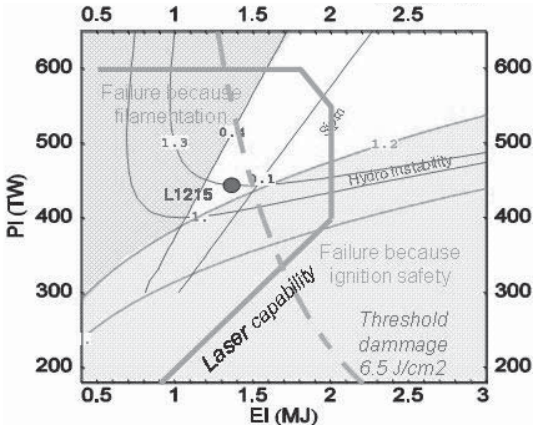

Fig. 8. Operative domain (Elaser, Plaser) at 3ω for constant aspect ratio and symmetry factor.

factors for laser-plasma instabilities (for example for filamentation) and for hydro-instability (it could be the in-flight-aspect-ratio). In Figure 8, at 3ω, the light-grey region is forbidden because the ignition safety factor is too low and the dark-grey region equally because of filamentation (we use a similar figure of merit for filamentation assuming a smoothing by KPP as Suter [13]). In between there is an operative domain at the "tip" of which you can see the L1215 target. It is interesting to note that the hydrodynamic stability factor could change only the "tip" of the domain (low laser energy).

We keep 20% margin with respect to the laser capability but the margin with respect to the optical damage threshold is very little (this threshold is 6.5 J/cm^2, today but we don't know it precisely because it depends on several factors among them the cumulated effect of the shots and the desired degree of quality of the optics).

We used the same approach with the global modelling before making any 2D simulations in order to find a domain if the LMJ was used at 2ω. For sake of simplicity, in a first step, we chose capsules homothetic to the 3ω capsules but bigger and employed with the same radiation temperature which can be varied from 250 eV to 300 eV in the domain. In this homothety all the capsule dimensions are multiplied by a factor h, so that the aspect ratio is conserved and if the radiation temperature is the same, the velocity is the same and the implosion time is multiplied by h. We impose the same safety factors as before, mainly S_{ign} and the filamentation factor. In particular that means that the 2ω laser intensity must be much lower than at 3ω, so the laser entrance hole must be larger: more laser energy at 2ω and larger hohlraum leads to a new trade-off for the operative domain. We came to the result that we need ∼2.2 MJ and 550 TW at 2ω or 2.7 MJ to get the same margin of 20%. For this target the homothetic factor is $h \sim 1.3$ with respect to L1215. It seems achievable for the laser technique point of view, if we use KDP converter optimized for 2ω (thicker than those used at 3ω). The laser capability is plotted in Figure 9 (3 MJ and 650 TW are the maxima according to the pulse duration). The optical damage threshold is roughly estimated to 9.5 J/cm^2 at

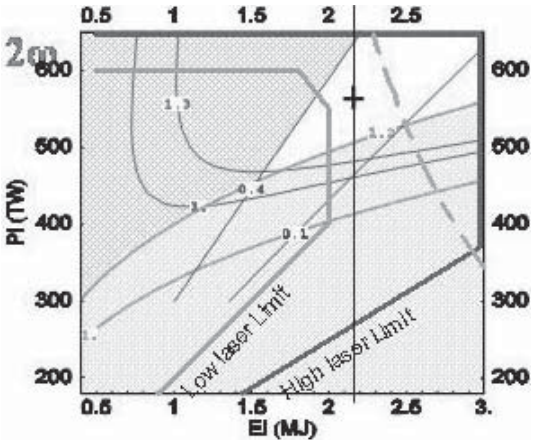

Fig. 9. Operative domain (Elaser, Plaser) at 2ω for fixed aspect ratio and symmetry factor.

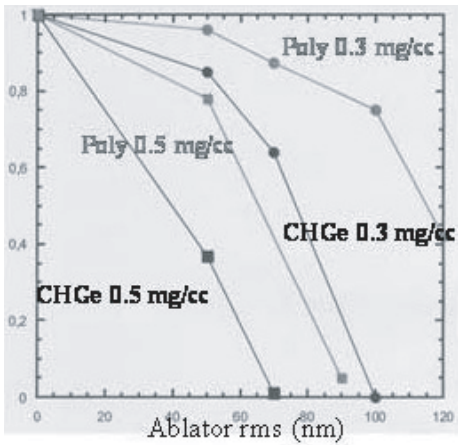

Fig. 10. YOC versus ablator roughness for our nominal capsule (curves labeled CHGe), for "new NIF-PT" (label Poly) and for two gas densities 0.3 mg/cc (circles) and 0.5 mg/cc (squares).

2ω, so at 2.2 MJ we have a slightly better margin than at 3ω regarding this issue. After having found a domain of target adapted at 2ω we are going to make 2D simulations to get more accurate predictions.

3.4 Sensitivity to the DT gas density

The DT gas density is related to the cryogenic DT temperature and so to the DT roughness. Our nominal capsule was designed to work at 18.4 K and with a DT gas density 0.3 mg/cc. In order to have a better DT roughness the temperature must be as close as possible to the triple point (19.7 K) but at the same time the DT vapour density increases (0.6 mg/cc at 19.7 K). Consequently the deceleration stage is delayed of a few 10 ps and the burn stage is modified such as the 1D burn robustness is degraded. It is not possible to re-optimize the deceleration with the same safety factors: we must increase the maximum radiative temperature T_r or modify the capsule.

So it is important to know how much the yield is degraded by the density increase by using multimode instability simulations as in Section 3.1. In Figure 10 we plotted the Yield-Over-Clean (YOC) versus the ablator roughness for our nominal capsule and two gas densities. Qualitatively we compared to calculations of a "new NIF-PT" (designed by Herrmann with a polyimide ablator 160 μm thick, DT 90 μm thick [14]) for two gas densities: the limit roughness is 60 nm at 0.3 mg/cc and 20 nm at 0.5 mg/cc and for NIF it is 100 nm and 50 nm respectively. The behaviour of both targets is very similar. It is interesting to notice that, in our simulations, the instability growth of high modes is not significantly modified by the gas density, therefore the gain degradation is due to less 1D implosion robustness.

3.5 A 1D diffusive mixing model

The multimode instability simulations are expensive in CPU time even in 2D, that is why it is interesting to have a chain of codes-&-models to calculate them after validating the chain on the 2D simulations. One chain can

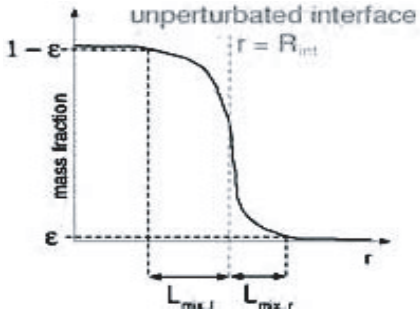

Fig. 11. Mass fraction in the mixing zone: the length L at the right is different to L at the left.

be composed of 2D simulation in the linear regime up to the ignition (quick simulation, no rezoning), a saturation model to get the right perturbation amplitude versus time [1]. The last stage of the chain is a 1D code where a mix model is implemented to calculate the yield. Here we described such a mix model and we compare the results to multimode FCI2 simulations.

The use of such a model is only possible when the dominant perturbation has a small wavelength. For LMJ gain capsule, we observed that the largest perturbations occur at the CH/DT interface (the convergence effect delayed the saturation), at least for our nominal capsule where the dominant mode is ∼80 high enough to justify the assumption of mixing-like effect on the yield. The hot spot perturbations are smaller because they are stabilized by ablation.

Our mix model, Medic is based on a 2 fluids description (not yet published): we solve a concentration equation and an energy equation with diffusive terms (no diffusion in momentum). The diffusion terms are proportional to the products LdL/dt where L is the RMS of the perturbations considered as a mixing length. It appeared that we must make the difference between the L_{mix_r} at the right of the interface and L_{mix_l} at the left. Of course the diffusion terms must be zero at the end of the mixing zone. In Figure 11 there is a scheme of the mixing zone.

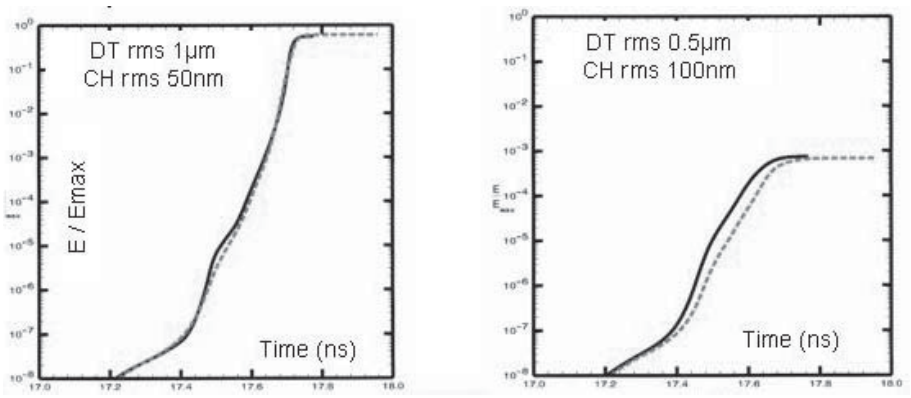

Fig. 12. Comparison of the normalized yield (fusion energy / total fusion energy for the target without perturbations) given by the mixing model (dashed curve) and the multimode FCI2 simulation (solid curve) for the nominal LMJ capsule (the time scale goes from 17.0 ns to 18, and the yield, from 10^{-8} to 1) : at the left with small initial CH roughness and at the right for large roughness (no gain).

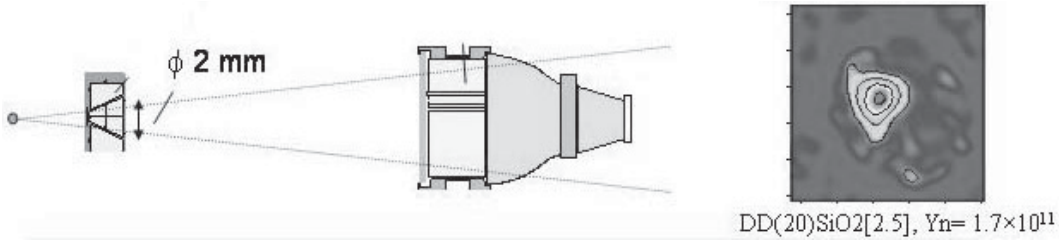

Fig. 13. Scheme of the neutron image system. Neutron image for a D+D reaction (yield is 10^{11} neutrons).

In Figure 12 we compare the yield history given by Medic and by FCI2 in 2 opposite cases: one with small roughness gives the nominal gain and the other one with large roughness does not ignite. The agreement is good over a 10^5–10^8 scale. In order to validate the process L was taken from the FCI2 simulations giving the yield, but in the future L must be given by a instability model and/or a set of single-mode 2D simulations.

4 Neutron diagnostics

4.1 Neutron image system

The penumbral neutron image technique of CEA is settled at Rochester and used for several years now on direct drive implosions [15]. The principle of the diagnostic is shown in Figure 13. The core images for capsules filled with D2 gas and low yield have been obtained, but with a poor resolution.

Images of capsules filled with DT gas have been successfully compared to X-ray images (Fig. 14) for yield larger than 10^{13} neutrons: the resolution is $\sim$25 μm.

LMJ requires a better resolution in the range 5–10 μm (the hot spot size is $\sim$30 μm and the DT size $\sim$70) that is why we replaced

(i) the conical aperture of the imaging system by a ring aperture;
(ii) the solid scintillator by an array of capillaries filled with a deuterated liquid (to improve also the sensitivity) [16].

The resolution extrapolated to LMJ conditions is 5–10 μm as expected and the signal-to-noise ratio is in the range 15–25.

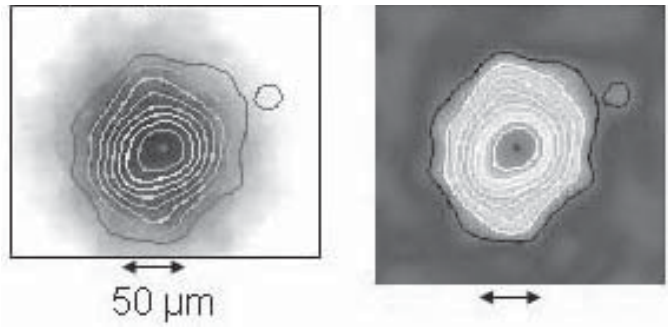

Fig. 14. Neutron image on the right and X-ray image (3–7 keV) at the left superimposed with neutron image contours showing a good agreement.

4.2 Time-of-flight spectrometer

The areal density is one of the important parameter of the burn. We developed at CEA a new neutron time-of-flight spectrometer insensitive to the gamma rays in order to detect the secondary high-energy neutrons (for D+D reactions) or tertiary neutrons (for D+T). From these in-flight-produced neutrons we can infer the areal density of the fuel.

The diagnostic is based on a converter neutron in proton and an avalanche of charges collected with micro strips [17].

In Figure 15 we show a first test of this device, namely a typical spectrum of secondary neutrons (12–16 MeV) measured at Rochester on a D+D implosion.

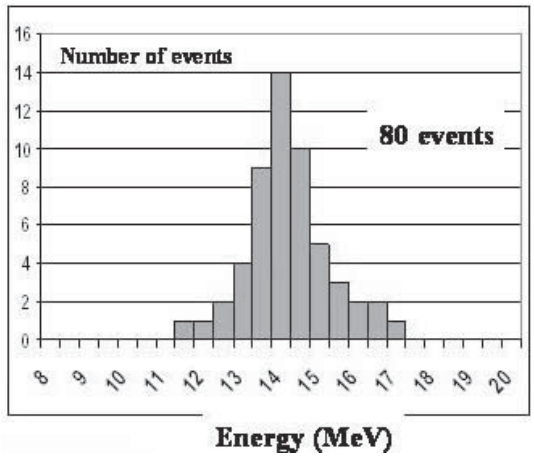

Fig. 15. Neutron spectrum obtained with the diagnostic Demin in a D+D implosion on Omega laser (horizontally the neutron energy in MeV, vertically number of counted events in arbitrary unit).

5 Conclusion

A lot of progress has been made in the target design for LMJ:

- the graded dopant improves the hydro stability and is compatible with the target fabrication;
- the filamentation figure of merit for laser plasma interaction has been added in our global modelling;
- a 2ω preliminary domain for LMJ has been given in the range 2–3 MJ, which is realistic for the laser point of view;
- the cumulated effects of all the low-modes asymmetries consolidate the specifications of LMJ for the nominal target L1215 at 300 eV. Without the mode 1 the DT deformation is small enough to get a significant gain with a very good probability, but the mode 1 could be an issue in the present status of our simulations.

A chain of hydro-code and laser propagation paraxial code shows that the longitudinal SSD of LMJ reduces the beam deflection. Another paraxial code with full hydrodynamics and Brillouin scattering and harmonics of the ion wave is now operative.

The hydrodynamic instability experiments are running with 2 radiographies routinely, but not completely interpreted.

For neutron images, today's results allow to extrapolate to the right resolution for LMJ (5–10 μm) and also to the right signal-to-noise ratio ($\sim$20).

References

1. P.A. Holstein et al., Nucl. Fusion **44**, S177 (2004)
2. D. Besnard, proceedings of IFSA'05 under publication
3. J. Lindl et al., Phys. plasmas **11**, 339 (2004)
4. G. Riazuelo, Phys. Plasma **7**, 3841 (2000)
5. M.L. Casnabet et al., Laser Part. beams **4**, 531 (1986)
6. R. Kauffman et al., Phys. Rev. Let. **73**, 2320 (1994)
7. J.L. Bourgade et al., Rev. Sci. Instrum. **72**, 1173 (2001)
8. P. Amendt et al., Phys. Plasma **4**, 1862 (1997)
9. R.E. Turner et al., Phys. Plasmas **10**, 2429 (2003)
10. M.M. Marinak et al., Phys. Plasmas **9**, 3567 (2002)
11. S. Haan et al., Phys. Plasma **12**, 056316 (2005)
12. R.C. Cook et al., Fusion technol. **35**, 224 (1999)
13. L. Suter, Phys. Plasma **11**, 2738 (2004)
14. S.W. Haan et al., *proceedings of IFSA'03*, edited by B. Hammel et al., Am. Nuc. Soc., IIlinois, M. Herrman, communication at IFSA'03, p. 55
15. L. Disdier et al., Rev. Sci. Instrum. **74**, 1832 (2003)
16. L. Disdier et al., Rev. Sci. Instrum. **75**, 2134 (2004)
17. M. Houry et al., *proceedings of Varenna summer school "advance diagnostics for magnetic and inertial Fusion"*, edited by A. Stott, A. Wootten (Kluver Acad. Plenum Publisher, 2002), p. 149